PERMAFROST AND PERIGLACIAL PROCESSES
Permafrost and Periglac. Process. (2015)
Published online in Wiley Online Library
(wileyonlinelibrary.com) DOI: 10.1002/ppp.1863

Late Quaternary Permafrost Distributions Downscaled for South America: Examinations of GCM-based Maps with Observations

Kazuyuki Saito,[1,2]* *Darío Trombotto Liaudat,*[3] *Kenji Yoshikawa,*[4] *Junko Mori,*[2,5] *Toshio Sone,*[6] *Sergey Marchenko,*[7] *Vladimir Romanovsky,*[7] *John Walsh,*[1] *Amy Hendricks*[1] *and Estefanía Bottegal*[3]

[1] International Arctic Research Center, University of Alaska, Fairbanks, Alaska, USA
[2] Japan Agency for Marine-Earth Science and Technology, Yokohama, Kanagawa, Japan
[3] El Instituto Argentino de Nivología, Glaciología y Ciencias Ambientales, CONICET, Mendoza, Mendoza, Argentina
[4] Water and Environmental Research Center, University of Alaska, Fairbanks, Alaska, USA
[5] National Institute of Polar Research, Tachikawa, Tokyo, Japan
[6] Institute of Low Temperature Science, Hokkaido University, Sapporo, Hokkaido, Japan
[7] Geophysical Institute, University of Alaska, Fairbanks, Alaska, USA

ABSTRACT

High-resolution maps of potential frozen ground distribution in South America have been produced for the present day (0 ka) and the Last Glacial Maximum (21 ka). Surface air temperature outputs from global climate models (GCMs) of the recent Paleoclimate Model Intercomparison Project were used for the reconstructions, and then downscaled from regional to local scales, with the help of a 1 arc-minute digital elevation model. Their validity was examined using fieldwork-based evidence and knowledge. The downscaled map for the present day successfully reproduces the presence of permafrost in the Andes, a task at which original coarse-resolution GCM output maps failed. The map also shows close correspondence with instrumental observations. Similarly, the downscaled distribution of 21 ka frozen ground shows overall consistency with geomorphological and/or palaeoenvironmental reconstructions. Areal coverage of potential permafrost for all of South America is estimated at 139 000 km^2 for today and 435 000 km^2 for 21 ka, mostly along the Andean mountain ranges. Regional inspections, however, show divergence from field-observed features, attributed to microclimatic effects and past permafrost conditions. For southern Patagonia, and especially the eastern lowlands, the diagnosed lower limit for permafrost is about 1000 m asl, whereas field evidence at lower altitudes indicates the presence of either permafrost or deep seasonal frost.

KEY WORDS: paleo-permafrost; South America; downscaling; Global Cliamte Modelling; geocryogeneic processes, PMIP3

INTRODUCTION

Understanding of the geographical distribution of frozen ground or periglacial phenomena in South America (e.g. ice or sand wedges, patterned ground and rock glaciers), as well as their variability through time, remains limited (notwithstanding the Andes Mountains) compared to that in the northern hemisphere (cf. Brown *et al.*, 1997; Vandenberghe *et al.*, 2014). Considerable effort has been devoted to aggregating fragmented field evidence, in order to delineate the areal extent of perennial and seasonally frozen ground, both today and during the Last Glaciation. The chronology of South American cryogenic features or landforms, however, has remained either unclearly defined or under debate. Further, field observations are sporadic and site-specific, and hindered by inaccessibility, especially in Patagonia or mountainous areas (Corte, 1953, 1986, 1991, 1997; Trombotto and Stein, 1993; Clapperton, 1993a; Schellmann *et al.*, 2000; Trombotto, 2002; Trombotto Liaudat, 2008). Previous efforts have included maps of land surface types in South America at the Last Glacial Maximum (LGM) (*c.* 18–20 ka for South America) compiled by Clapperton (1993a), including a northern limit for seasonally or perenially frozen ground, present-day cryogenic activities based on climatic conditions (e.g. mean annual air temperature (MAAT)) by Trombotto (1991, 2000) and regional interactions between creeping

*Correspondence to: K. Saito, International Arctic Research Center, University of Alaska Fairbanks, Fairbanks, Alaska, USA. E-mail: ksaito@iarc.uaf.edu

Received 25 December 2014
Revised 6 July 2015
Accepted 6 July 2015

permafrost, occurrence of ground ice and cryogenic processes by Trombotto (2003). These maps, however, generally remain qualitative or regional.

Global climate models (GCMs) or, more recently, Earth System Models can provide physically consistent representations of the entire South American climate and ecosystem. An international community effort – the Paleoclimate Model Intercomparison Project, Initiative III (PMIP3) – simulated Late Quaternary global climates (Braconnot *et al.*, 2012), which constitute the physical science basis of chapter 5 of the most recent Intergovernmental Panel on Climate Change (2013) report. This PMIP3 reconstruction showed better matching with observation-based knowledge than did the previous PMIP2 (Braconnot *et al.*, 2007), due to finer horizontal resolution (roughly from the level of 2.5° to 1.0°) and more realistically simulated climatology (e.g. in the western half of Eurasia by Saito *et al.*, 2013a). However, the resolved spatial scale and processes implemented are still insufficient for direct comparisons with field observations. To resolve this gap, downscaling methodologies have been developed utilising (1) a statistical classification with air freezing and thawing indices, and/or (2) topographical downscaling using a digital relief model and atmospheric lapse rate (e.g. Levavasseur *et al.*, 2011; Fiddes and Gruber, 2014; Saito *et al.*, 2014). Saito *et al.* (2014) successfully mapped complex regional distributions of seasonal and multi-year freezing in north-eastern Asia.

In this study, we aim to produce the first physically consistent, high-resolution maps of frozen ground distribution for all of South America during the Late Quaternary using this tested downscaling technique, and to examine them using fieldwork-based knowledge and evidence (e.g. Trombotto, 2002; Trombotto Liaudat, 2008) for validations and discrepancy analysis. Analysis was conducted for the three Late Quaternary periods: 0 k (pre-industrial), the mid-Holocene and the LGM. The 0 ka simulations use orbital conditions at 0 ka (i.e. 1850), interpreted practically as a modern reconstruction for this study. The mid-Holocene, or Holocene Climatic Optimum, is simulated for around 6000 years before present (similarly, '6 ka'), and '21 ka' simulations use conditions for the northern hemisphere LGM. All simulation data were taken from the PMIP3 data archives (e.g., http://pcmdi9.llnl.gov/esgf-web-fe/).

In the following sections, reconstructed distributions are compared, evaluated and discussed in terms of surficial distribution, latitude-altitude relationships and longitude-altitude cross-sections at selected parallels.

DATA AND METHODS

Digital topographic data ETOPO1 (Amante and Eakins, 2009) were used to determine the distribution of surface elevation (Figure 1A). The horizontal resolution of ETOPO1 is 1 arc-minute (approximately 1.85 km in latitude and longitude at the equator). The domain of this analysis was the rectangular area of 60°S–10°N in latitude and

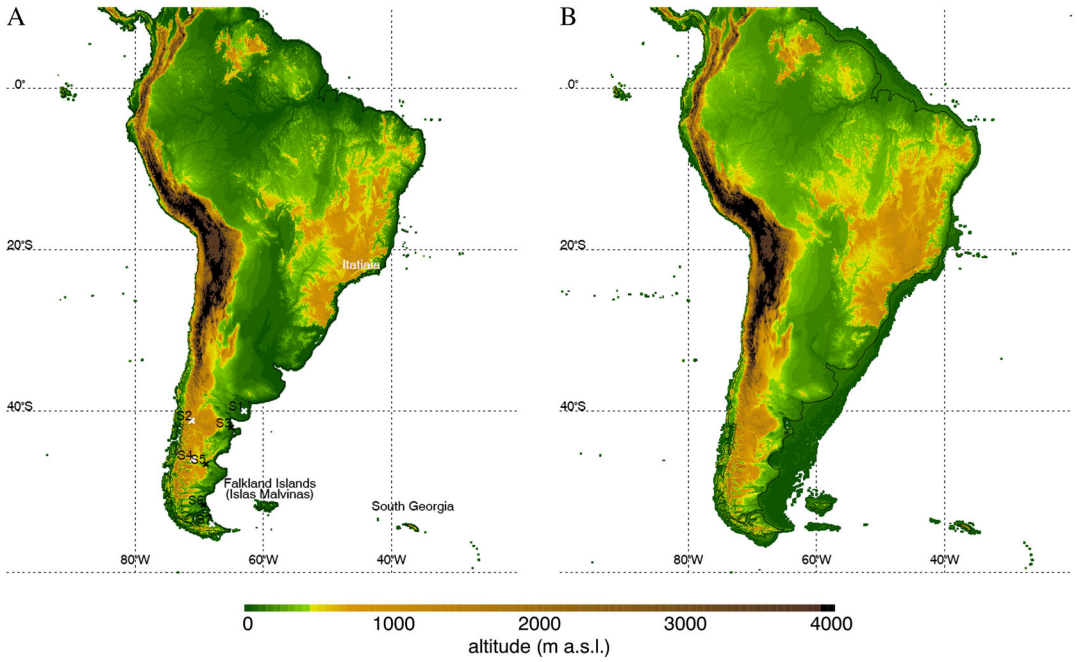

Figure 1 Topography of South America examined in this study for (A) the present day and (B) the Last Glacial Maximum period, for which sea level is lowered by 127 m. Colours show altitude (m asl). In (B), the modern coastline is drawn as a thin black line for reference. Explanations of sites (S1–S7) are given in Table 2. This figure is available in colour online at wileyonlinelibrary.com/journal/ppp

100°W–20°W in longitude, covering the entire South American continent and adjacent islands. In order to estimate the altitudes of the continent at the time of the LGM (Figure 1B), the change in sea level at the LGM was set to -127 m, taken from the latest eustatic estimation (Clark and Mix, 2002; Milne and Mitrovica, 2008). Glacial isostasy, an important factor in considering local to regional topography on glacial-interglacial timescales, was not taken into account in this study because of uncertainties and limitations in the currently available isostatic data with respect to the locations and resolutions in the continental area (Milne and Mitrovica, 2008).

Geophysical values for PMIP3 models used for the 0 ka and 21 ka periods, as well as their relevant information (e.g. horizontal resolutions, individual names) used in this study, are summarised in Table 1 of Saito *et al.* (2013a). For 6 ka, this relevant information is also given in Table 1. Surface air temperature at 2 m was used for downscaling and diagnosis of the subsurface thermal regime. Monthly surface air temperature data derived by the Climatic Research Unit (CRU) TS3.20 (University of East Anglia Climatic Research Unit *et al*., 2013) were used as a modern reference for observation-based air temperature in the region. Since horizontal resolution from model outputs and CRU data differ from one another, surface air temperature was shifted first to mean sea level using the atmospheric lapse rate value of -6.5 °C/km, then interpolated and re-gridded for a common resolution of 288 grids (1.25° interval) by 192 grids (*c.* 0.94° on average), before analysis for mutual comparison. Downscaling was done by interpolation to ETOPO1 grids and shifting back to the corresponding altitude, using the same atmospheric lapse rate value. Examination of the distribution of the simulated atmospheric lapse rates from the surface to 400 hPa in the lowlands (below 1500 m asl) and uplands (above 1500 m asl) in South America showed that the lapse rate used was in good accordance both with the present day (annual range of model averages was -6.18 to -6.96 °C/km for the lowlands and -6.62 to -6.88 °C/km for the uplands) and the LGM (similarly, -6.13 to -6.84 °C/km for the lowlands and -6.83 to -7.02 °C/km for the uplands). Sensitivity of the reconstruction to choice of the atmospheric lapse rate is discussed in the Latitude-Altitude Relationship section (cf. discussion on lapse rate sensitivity in northeastern Asia by Saito *et al.*, 2014). Freezing and thawing indices were then computed from monthly values, in the same manner as defined by Saito *et al.* (2014, equations 1–2).

Types of frozen ground were classified by freezing and thawing indices (I_f and I_t, respectively, in degree-days Celsius) into the following five categories, from the method described by Saito *et al.* (2014, equations 3–7): climate-driven permafrost (CP: $I_t < 0.91I_f - 2300$), corresponding to 'continuous permafrost'; environmentally conditional permafrost (EP: $0.9I_t - 2300 < I_t < 2.4I_f - 3300$), corresponding to 'discontinuous permafrost'; seasonal frost (Sf: $(2.4I_f - 3300 < I_f) \wedge (30 < I_f)$) for deep and/or long-lasting seasonally frozen ground; intermittent frost (If: $0 < I_f < 30$) for a short duration (i.e. less than 2 weeks) freezing; and Nf ($I_f = 0$) for 'no freezing' (Saito *et al.*, 2013a, 2014). Areas of known distribution of glaciers, ice caps, ice fields and/or ice sheets are shown as 'land ice'.

Sites of active or past *in-situ* permafrost used for examination of Holocene and Late Pleistocene reconstructions are listed in Tables 2 and Supplementary Table 1. Also described here are cryogenic features such as frost crack structures or thermal contraction cracking, ice-wedge

Table 1 Summary of PMIP3 model simulations for 6 ka (mid-Holocene, or Holocene Climatic Optimum).

Model	Horizontal resolution (land)	Modelling centre (or group)
CCSM4	288 × 192	National Center for Atmospheric Research
CNRM-CM5	256 × 128	Centre National de Recherches Météorologiques / Centre Européen de Recherche et Formation Avancée en Calcul Scientifique
CSIRO-Mk3-6-0	192 × 96	Australian Commonwealth Scientific and Industrial Research Organization Marine and Atmospheric Research (Melbourne, Australia) in collaboration with the Queensl and Climate Change Centre of Excellence (Brisbane, Australia)
GISS-E2-R	144 × 90	NASA Goddard Institute for Space Studies
HadGEM2-ES	192 × 145	Met Office Hadley Centre
IPSL-CM5A-LR	96 × 96	Institut Pierre-Simon Laplace
MIROC-ESM	128 × 64	Japan Agency for Marine-Earth Science and Technology, Atmosphere and Ocean Research Institute (The University of Tokyo), and National Institute for Environmental Studies
MPI-ESM-P	192 × 96	Max-Planck-Institut für Meteorologie (Max Planck Institute for Meteorology)
MRI-CGCM3	320 × 160	Meteorological Research Institute

Simulations for 0 ka (pre-Industrial) and 21 ka (LGM) are summarised in Saito *et al.* (2013a). PMIP3 = Paleoclimate Model Intercomparison Project, Initiative III; LGM = Last Glacial Maximum.

Table 2 Comparison between observed and simulated values of MAAT in Patagonia.

#	Locality	Lat (S)	Lon (W)	Altitude	MAAT obs.	MAAT (0 ka)	MAAT CRU	MAAT (21 ka)	Δ (21-0)
S1	Viedma	40°48'	62°59'	6 m	14.1 °C	12.8 °C	13.6 °C	11.1 °C	−1.7 °C
S2	San Carlos de Bariloche	41°09'	71°10'	840 m	7.9 °C	5.8 °C	3.4 °C	2.1 °C	−3.7 °C
S3	Puerto Madryn	42°46'	65°02'	7 m	13.5 °C	11.7 °C	11.6 °C	9.8 °C	−1.9 °C
S4	Estancia Valle Huemules	45°57'	71°31'	650 m	5 °C	4.1 °C	3.6 °C	−0.3 °C	−4.4 °C
S5	Las Heras	46°33'	68°57'	332 m	9.9 °C	7.1 °C	7.4 °C	3.8 °C	−3.3 °C
S6	Río Gallegos	51°62'	69°20'	20 m	7.1 °C	5.2 °C	5.7 °C	−0.6 °C	−5.8 °C
S7	Ushuaia	54°48'	68°18'	16 m	5.5 °C	4.6 °C	4.2 °C	−2.6 °C	−7.2 °C

Directly observed values (MAAT obs.) were taken from Table 2 in Trombotto Liaudat (2008). MAAT CRU is interpolated and downscaled from the observation-based CRU data-set. Simulated values MAAT (0 ka) and MAAT (21 ka) are averages from among the models. Locations of these sites are denoted in Figure 1. MAAT = Mean annual air temperature; CRU = Climatic Research Unit (University of East Anglia).

pseudomorphs, sand-wedge casts, composite-wedge casts and rock glaciers (French, 2007; Bockheim *et al.*, 2009). These landforms as well as other processes in South America (e.g. patterned ground, gelifluction and thick taluses) indicate intense freezing occurring at the sites (Corte, 1986; Clapperton, 1993a; Trombotto, 2000; Trombotto Liaudat, 2008). However, a clear distinction between permafrost (temperature at or below 0 °C for at least two consecutive years) and seasonal freezing (freezing in winter while thawing completely in summer, implying a large seasonal temperature range) is not easy, especially for the dry climate of southern Patagonia, as 'seasonal freezing may be adequate for the development of polygonal cracking' (Clapperton, 1993a, p. 522).

Sea ice concentration output data were also used to determine the northern limit of Antarctic winter sea ice extent, defined as areas with more than 15 per cent sea ice concentration in September at the LGM (19.5–16.0 ka; Gersonde *et al.*, 2005).

RESULTS AND DISCUSSION

Downscaled Surface Air Temperature and Frozen Ground

Local comparisons of the MAAT at field sites (S1–S7, Table 2) in Patagonia and Tierra del Fuego (locations marked in Figure 1A) show that the downscaled simulation output (column 7 in Table 2; MAAT (0 ka)), the downscaled observation-based data-set (MAAT CRU; column 8) and direct observation (MAAT obs.; column 6) are reasonably consistent with one another, while modelled temperature (MAAT (0 ka)) and the climate data-set (MAAT CRU) tend to be cooler than local observations (MAAT obs.). The simulated differences in temperature between the present day (MAAT (0 ka)) and the LGM (MAAT (21 ka)) are negative at all sites (Table 2; Figure 2B), with a margin of difference greatest at either higher elevation or a more southerly location (column 10 in Table 2). Using data at cryogenic sites, Garleff and Stingl (1986), Trombotto (1994, 1996) and Corte (1997) showed that much larger decreases – for instance, between 10 and 15 °C – were possible between modern and LGM temperatures at some sites. They considered the difference between MAATs in Patagonia today, as well as the temperatures required for cryogenic structures to build, which also depend on the host material. To build ice wedges in Patagonian sediments, for example, requires MAATs below -3.5 °C (cf. Péwé, 1969; Romanovskij, 1973; Corte, 1997).

The downscaled MAAT for 21 ka ranged from 25 °C in some equatorial areas to -25 °C in the Central Andean mountain ranges (Figure 2A), though it remained lower than today for the entirety of the region studied here (Figure 2B).

In the tropical to subtropical lowlands, the decrease in surface air temperature showed a range of 2–4 °C (Figure 2B). The Brazilian Highlands were cooler by 3–4 °C than today. In the mountain ranges, the MAAT dropped by 2–4 °C in the Central Andes and by 4–7 °C in southern Patagonia and Tierra del Fuego. Pollen-based palaeoclimatic reconstructions show that during the Late Pleistocene glaciation, the MAAT was lower everywhere in Central and South America, both in the Andean high areas and lowlands, ranging from 4 to 5 °C cooler (Markgraf, 1989), although with a somewhat warmer summer (leading to a greater seasonal amplitude), especially east of the Andes (Markgraf, 1991). In southernmost South America, biogeographic and geologic evidence suggests that the MAAT was apparently cooler by as much as 7–8 °C (Heusser, 1991, 2003; Benn and Clapperton, 2000). The downscaled MAAT shows results largely consistent with evidence-based reconstruction.

Table 3 Statistics for surficial areal extent (in 10^3 km^2) underlain by different types of frozen ground in (a) the entirety of South America (60°S–10°N) and (b) Patagonia and Tierra del Fuego (60°S–37°S) among model simulations.

Era (ka)	Frozen ground type	Min	Median	Max	Mean	SD	Mode	CRU
South America (60°S–10°N)								
0	Nf	15638	15961	16303	16010	269	16110	16560
0	If	469	512	626	521	61	322	676
0	Sf	772	1174	1402	1096	253	1214	521
0	EP	67	98	166	116	43	110	21
0	CP	17	26	110	42	39	29	6
	(total)						17785	17784
6	Nf	15763	16103	16400	16088	233	16132	—
6	If	379	537	658	527	95	397	—
6	Sf	690	990	1406	1059	237	1167	—
6	EP	22	70	179	80	48	66	—
6	CP	6	25	94	30	29	23	—
	(total)						17785	
21	Nf	15961	16838	17108	16602	423	16662	—
21	If	557	801	1189	824	236	685	—
21	Sf	1613	1832	2159	1860	194	2016	—
21	EP	155	362	483	338	121	262	—
21	CP	53	112	324	164	104	163	—
	(total)						19788	
Patagonia and Tierra del Fuego (60°S–37°S)								
0	Nf	337	522	823	594	201	662	715
0	If	308	360	379	347	32	213	486
0	Sf	206	495	724	441	217	508	193
0	EP	3	10	23	11	8	10	1
0	CP	0.4	2	4	2	2	2	0.1
	(total)						1395	1394
6	Nf	420	606	679	569	98	596	—
6	If	228	292	480	322	84	291	—
6	Sf	264	491	702	492	158	499	—
6	EP	3	7	21	10	7	7	—
6	CP	0.4	2	4	2	1	1	—
	(total)						1395	
21	Nf	52	423	535	320	200	276	—
21	If	388	579	764	552	134	580	—
21	Sf	998	1248	1451	1227	167	1300	—
21	EP	50	150	225	127	67	82	—
21	CP	14	45	77	41	25	28	—
	(total)						2267	

Nf = No freezing; If = intermittent frost; Sf = seasonal frost; EP = environmentally conditional permafrost; CP = climate-driven permafrost; CRU = Climatic Research Unit (University of East Anglia).

Figure 3 shows maps of downscaled frozen ground distribution reconstruction derived from GCM-simulated freezing and thawing indices for the 0 ka (Figure 3A) and 21 ka (Figure 3B) periods. The mode (most frequent entities) of classification type for each grid was taken as representative among the models. Areas known to be potentially entirely or partially covered by ice bodies, such as glaciers, ice caps, or ice sheets are shown by yellow patches for the present day (Figure 3A), based on the World Glacier Inventory (World Glacier Monitoring Service and the National Snow and Ice Data Center, 1999, updated 2012), and by yellow hatching for the LGM (Figure 3B), integrated from previous knowledge (Schubert and Clapperton, 1990; Clapperton, 1993a; Hulton *et al.*, 2002; Heusser, 2003; Coronato and Rabassa, 2007).

It is worth mentioning that the presence of South American permafrost (in the Andes) for 0 ka appears correctly in Figure 3A, whereas the original coarse-resolution global map (that is, before downscaling) mostly fails to resolve it (Figure 3C). For the present day, permafrost extent is limited to the highest parts of the Central and Southern Andes and Tierra del Fuego. A detailed regional examination of the Central Andes near Mendoza is shown in Figure 4A. The downscaled map is consistent with

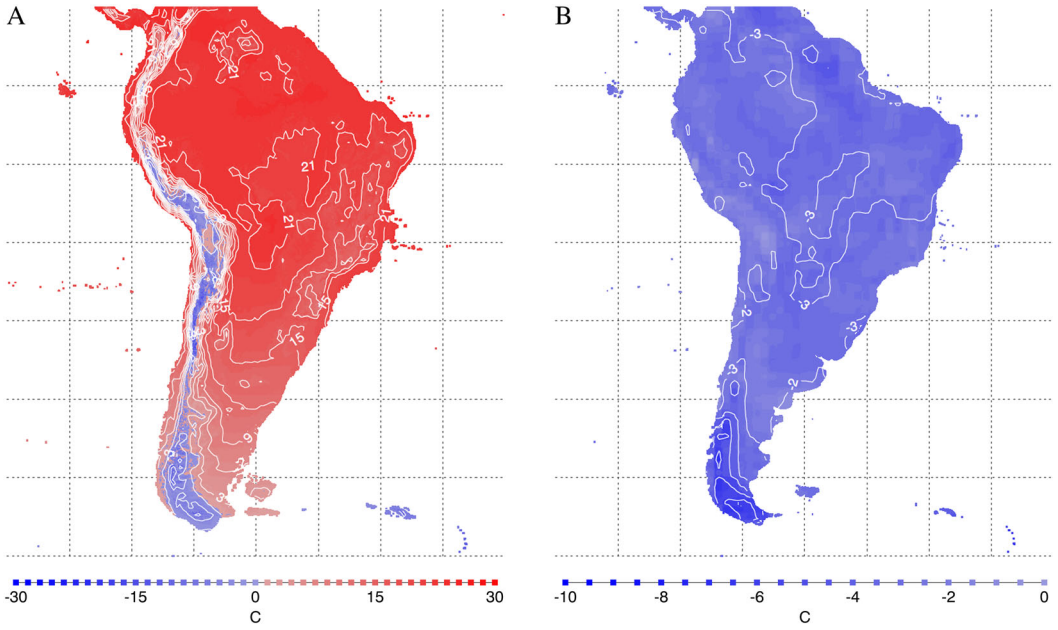

Figure 2 (A) Mean annual air temperature in South America at 21 ka and (B) differences from present-day (0 ka) values (i.e. 21 ka - 0 ka). This figure is available in colour online at wileyonlinelibrary.com/journal/ppp

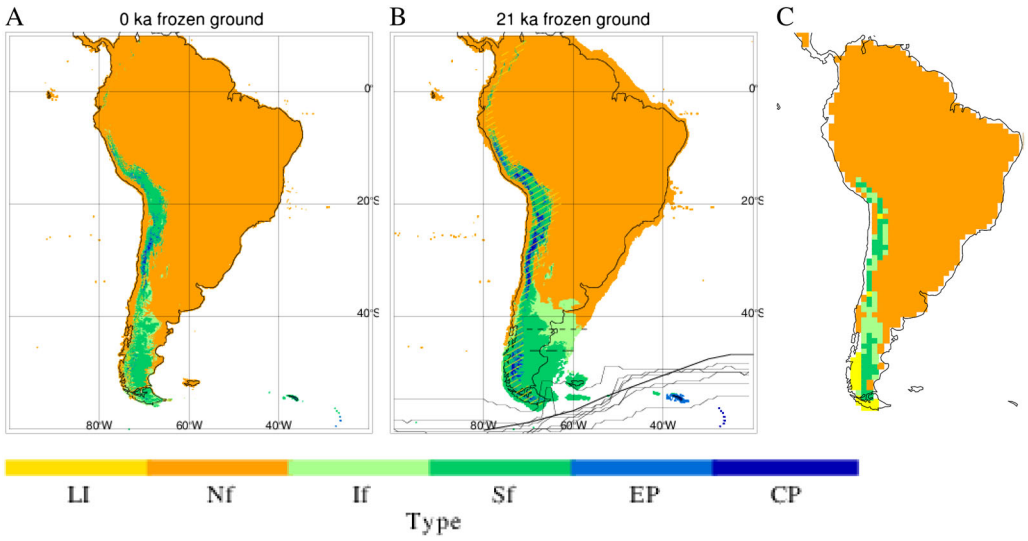

Figure 3 Downscaled frozen ground distributions, derived from PMIP3 models and an ETOPO1 digital elevation model for (A) 0 ka and (B) 21 ka. Hatches in the 21 ka panel show estimated areas covered by glaciers and ice caps. The colour scheme shows land ice (glaciers, ice caps; LI: yellow), no freezing (Nf: orange), intermittent frost (freezing shorter than 2 weeks; If: pale green), seasonal frost (Sf: green), discontinuous permafrost ('environmentally conditional permafrost' in Saito *et al.* (2013a); EP: pale blue) and continuous permafrost ('climate-driven permafrost'; CP: blue). In (B), winter sea ice extent (September sea ice concentration $> 15\%$) is drawn as solid lines, where thin lines show the result of individual models and thick lines show reconstruction (Gersonde *et al.*, 2005). The dashed line at 42°S denotes the northern limit for seasonally frozen ground at the Last Glacial Maximum (LGM) after Clapperton (1993a), and the long dashed line near 46°S denotes that for permafrost after Trombotto Liaudat (2008). (C) Distribution of current frozen ground at the original common horizontal resolution (288 grids in longitude by 192 grids in latitude). PMIP3 = Paleoclimate Model Intercomparison Project, Initiative III. This figure is available in colour online at wileyonlinelibrary.com/journal/ppp

fieldwork evidence, though much of the field data comes from the border between perennially and seasonally frozen ground. Additional discussion is offered in the Longitudinal Cross-Section section.

At 21 ka, areas of permafrost extended to the north and south in the Andes, also spreading slightly into the southern Patagonia and Tierra del Fuego regions (Figures 3B and 4B). In the Brazilian Highlands, the Itatiaia massif (location

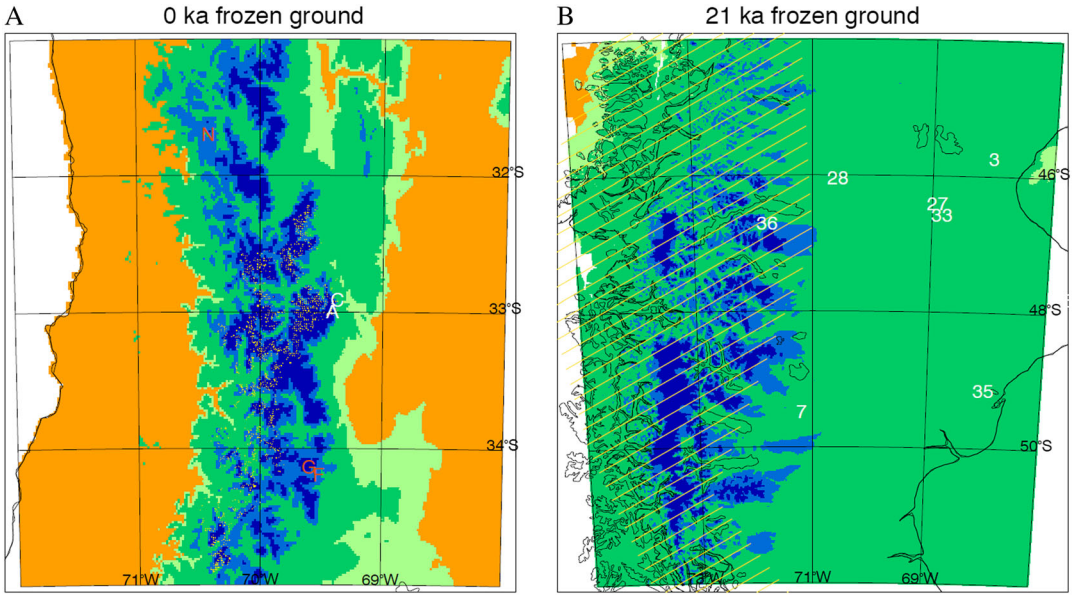

Figure 4 Local comparison of downscaled frozen ground distribution for (A) 0 ka (35°S–31°S, 68°W–72°W) and (B) 21 ka (44°S–52°S, 67°W–75°W). The colour scheme is the same as given in Figure 3. Evidence is based on field observations for 0 ka and 21 ka, and summarised in Table 2. Sites shown with white characters or numbers denote susceptibility to permafrost or deep seasonal freezing, while those with red denote the presence of seasonal freezing (Table 3). This figure is available in colour online at wileyonlinelibrary.com/journal/ppp

shown in Figure 1A), with a plateau higher than 2000 m, presents a possible location, if one exists, of solifluction activities during the LGM period (see Modenesi, 1992). There has been no evidence so far, however, to support that activity during this period (cf. Clapperton, 1993a, 1993b), and no permafrost was diagnosed in the Brazilian Highlands in the downscaled map, with only Sf to If above 2500 m asl (Figure 3B cf. Figure 6B).

Clapperton (1993a), aggregating various evidence and sources, drew a northern limit for seasonally frozen ground at the LGM around 42°S, noting the presence of permafrost to the south of the San Jorge Gulf (45°S–46°S), on the basis of tundra polygons and ice-wedge casts (cf. Clapperton, 1993a, Figure 23.10). Figure 3B here shows If appearing along the Atlantic coastline, to the south of 42°S, and seasonally frozen ground around 46°S (Figure 4B). No extensive permafrost was diagnosed in the Patagonian lowland, however. Further, regional examination from recent fieldwork shows that sites with frost crack structures and/or cryoturbation spread southward from around 46°S (e.g. Trombotto and Stein, 1993; Trombotto, 2002; Trombotto Liaudat, 2008). Recent studies (Goyanes and Massabie, 2015) about push moraines in the upper valley of the Santa Cruz River (*c*. 51°15'S, 71°45'W) and the drainage of meltwater from Pleistocene ice in west Patagonia support the permafrost model proposed by Trombotto (2002). These phenomena are indeed quite indicative of the presence of permafrost, though they can still occur under deep seasonal frost conditions, especially when the environment is very dry.

The South American continent shows high precipitation contrasts, especially between the eastern and western sides of the Andes. The median ratio of simulated precipitation on the eastern side to that on the western side among the models was 41.7 per cent for the 18°S–23°S band and 6.1 per cent for the 42°S–47°S band for 21 ka, and 44.3 per cent and 13.3 per cent for 0 ka, respectively. A moisture reconstruction by Markgraf (1989) suggested that moisture was very limited in the continent before 12 ka, at up to just 50 per cent of today's amount, except for the southern subtropics (locations between 20°S and 38°S) and the western side of the Southern Andes (43°S to 54°S), where it was greater. Simulated LGM precipitation averaged over the above-mentioned latitudinal bands decreased by 6.4 per cent for 18°S–23°S and by 12.5 per cent for 42°S–47°S. The frozen ground classification scheme applied in this study, derived from present-day observations and climate conditions, may not be directly applicable in some parts of South America at the LGM due to overall drying and the strong contrast between wet and dry conditions (see the discussion below). Nevertheless, the reconstructed frozen ground distribution does not contradict the empirical knowledge mentioned above, considering that the areas of downscaled permafrost are limited to the mountains, with probable thick snow or ice (shown by hatches in Figure 3B), and that these areas do not extend to the Atlantic coastline, though effects of extreme moisture contrast on frozen ground distributions do deserve further investigation.

In contrast, it is reported that the present-day Falkland Islands (Islas Malvinas) show only 'modest geocryogenic activities' (Clapperton, 1993a, p. 546), such as shattered bedrock, active solifluction lobes and ploughing blocks, at altitudes greater than 500 m due to a cool, sub-humid climate. This activity was presumably more extensive in

the Late Pleistocene glaciation period (including the LGM), despite a lack of chronological control (Clapperton, 1993a; Hall, 2002). Downscaled modelled distribution, however, shows no cryogenic activities in the islands for today, and only Sf for 21 ka (Figure 3B).

Following the above results, we examined the possible influence of simulated Antarctic sea ice extent on air temperature in southeastern Patagonia. It is known for the northern hemisphere that LGM permafrost simulation is very sensitive to Arctic sea ice extent (Vandenberghe *et al.,* 2012). If simulated sea ice is reduced from its actual distribution during the LGM period, this may result in a warm bias for the region. The northern limits for winter sea ice extent in the Drake Passage, either reconstructed from siliceous microfossils (Gersonde *et al.*, 2005) or modelled, are illustrated in Figure 3B. The reconstructed northern limit (thick line) extends further to the north than any model simulation (thin lines) in the 35°W–20°W sector, but it more or less coincides within the 80°W–40°W sector with those simulated. Also, no systematic correspondence was found between the position of the northern limit of ice and the extent of downscaled areas diagnosed as permafrost (not shown).

Another possibility for discrepancy is insufficiency in the frozen ground classification methodology, especially in terms of accounting for the effect of the very dry climate. The method used was based on the present-day northern hemisphere climate and frozen ground distribution, especially those in the USA, Russia, China and Mongolia (Saito *et al.*, 2014). These sites may not have samples representing an LGM Patagonian climate that is very dry but not extremely cold, in comparison to the dry and cold coastal tundra of the North Slope of Alaska or coastal Siberia today. This remains a theme for future research.

The statistics for downscaled areal extent for each frozen ground type for 0 ka, 6 ka, and 21 ka are summarised in Table 3 for all of South America, and for the regions of Patagonia and Tierra del Fuego. Note that this summary does not include the presence of glaciers or large ice sheets, but only classifies the potential subsurface thermal regime, given air temperature conditions near the surface. Areal extent in Table 3, therefore, should be understood as maximum coverage, including those areas that are (were) covered by large ice bodies in reality (and, hence, had a different thermal regime than diagnosed). The extent of perennial ice body coverage, however, remains poorly understood or documented, requiring understanding of the simultaneous conditions of both low temperature and sufficient moisture supply for ice fields to build up substantial ice bodies (Clapperton, 1993b). Yet, we are presented with very arid conditions here, except for the humid Andes south of 35°S and their western flank south of 43°S. A modelled LGM reconstruction gives an areal coverage of 91 872 km^2 for the Northern Patagonian ice sheet (Hubbard *et al.*, 2005), for example, and ice sheet coverage exceeding 500 000 km^2 along the Andes south of 38°S (from Hulton *et al.*, 2002, assuming an average thickness of 1000 m). For reference, present-day ice coverage estimates are given for Patagonian ice fields (Hielo Patagónico Norte and Hielo Patagónico Sur) as 17 200 km^2 (Skvarca, 2002), or for perennial ice cover south of 35°S as 20 400 km^2 (Trombotto Liaudat, 2008, after Lliboutry, 1998). That said, the potential 21 ka permafrost area (435 000 km^2, the sum of CP and EP was about three times that of the present day (139 000 km^2) for all of South America. In Patagonia and Tierra del Fuego, the total area potentially underlain by permafrost at 21 ka was about 110 000 km^2, or more than nine times the modern extent (12 000 km^2), of which a certain part was definitely covered by LGM glaciers or ice sheets.

Latitude-Altitude Relationship

Clapperton (1993a) estimated that the equilibrium line altitude along the Andes at the LGM descended by 800 m or more both at the equator and Patagonia, compared to today. In the equatorial region, this figure was between 800 and 1100 m, where the western cordillera (and western side) showed a smaller descent than the eastern cordillera (eastern side). The altitude of cryogenic activities should have descended accordingly, though the lowering may not necessarily be the same as that of snow lines, due to other local conditions such as temperature, precipitation, aspect and micro-topography (Corte, 1986; Clapperton, 1993b; Saito *et al.*, 2013b). Figure 5 shows the latitude-altitude cross-section of downscaled, simulated frozen ground distribution for 0 ka and 21 ka. Overlaid dashed lines in the figures represent the lower limit of cryogenic activities for each period, estimated by Corte (1986) and modified by Clapperton (1993a). The modern limit runs parallel (but constantly lower by 200–400 m south of 20 °S) to the boundary between simulated permafrost (blue) and seasonally frozen ground (green) zones. The lower limit, estimated from more recent fieldwork in Patagonia (Table 1 in Trombotto Liaudat, 2008), however, coincides better with the simulated boundary. Site observations in the Central Andes (31°S–35°S), marked by the same site characters as in Figure 4 and Supplementary Table 1, also demonstrate better correspondence with the downscaled modelled distribution. In the subtropics (16°S–0°S), direct observation of borehole temperatures indicates that there is no permafrost found below 5000–5200 m asl, except for rock glaciers, a finding also consistent with Figure 5A.

By contrast, the lower limit of cryogenic activities for the LGM estimated by Corte (1986) and Clapperton (1993a) showed a larger discrepancy, of up to 1000 m or more, from the permafrost boundary in the downscaled reconstruction. Rather, the estimated limit line runs along the upper limit of the downscaled If (pale green) or Nf (orange) zones. Reasons for this discrepancy, other than discussed above, remain unclear. The estimation line, possibly suffering from insufficient evidence or inadequate interpretation, or both, may be improved with the aggregation of more recent evidence. Further, the timing for permafrost to reach maximum extent in South America

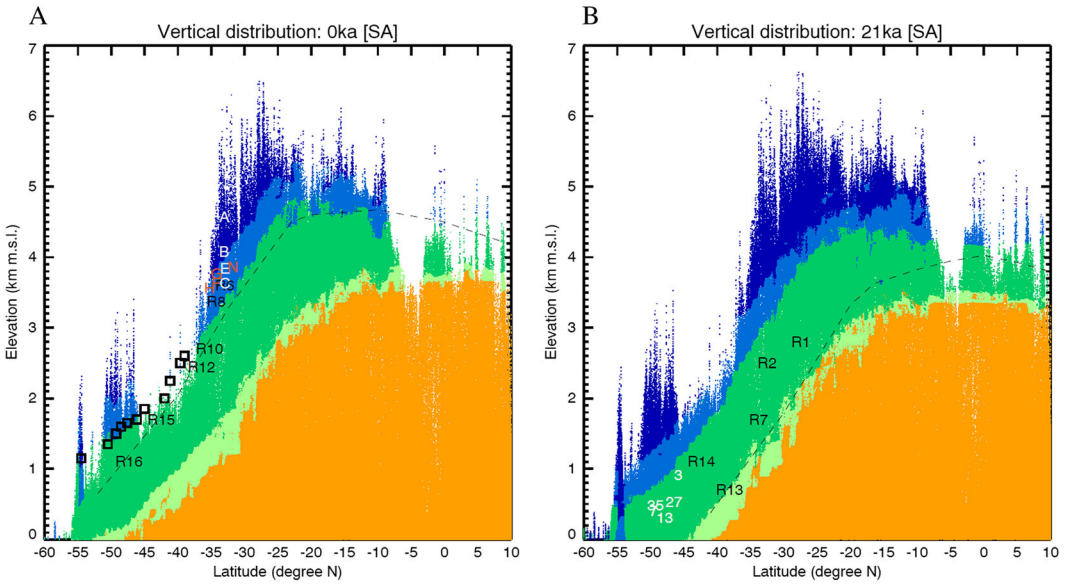

Figure 5 Latitude-altitude cross-section of frozen ground distribution for (A) 0 ka and (B) 21 ka periods. The colour scheme is the same as given in Figure 3. Characters and numbers in white denote sites susceptible to permafrost or deep seasonal freezing, while those in red show no freezing activity (Table 3). Lower limits for present-day mountain permafrost (squares in the left figure) are taken from Table 1 of Trombotto Liaudat (2008). Dashed lines show the lower limits of intense cryogenic activity (after Corte, 1986; Clapperton, 1993a). Rock glaciers (shown here as R1, R2, ...) as indicators of current and LGM permafrost are explained in the text and Supplementary Table 1. This figure is available in colour online at wileyonlinelibrary.com/journal/ppp

may have differed from 21 ka. Despite these discrepancies, the simulation- and observation-based latitudinal gradient of the limits matches well.

As stated in the Data and Methods section, the atmospheric lapse rate was held constant at -6.5 °C/km for both 0 ka and 21 ka in this study. The overall range of average lapse rates among the models is -6.13 to -7.02 °C/km, where values for 'uplands', 'winter' and 'LGM' tend to be higher than for other cases, implying that the current method may overestimate the altitude of the permafrost-seasonally frozen ground boundary. Nevertheless, intra-model distributions are narrow (the typical standard deviation is 0.91 for lowlands and 0.44 for uplands), and similar to each other. Sensitivity examinations in the range of -4.5 to -8.5 °C/km showed that the resulting areas of LGM reconstruction varied linearly against the lapse rate, and that the gradient was 24.7×10^3 km^2 for EP and 91.6×10^3 km^2 for CP for a change of 1.0 °C/km for the entire South America. These values were found to be smaller than the variations in the diagnosed areas among model simulations (cf. inter-model standard deviation for entire South America at the LGM is 121.4×10^3 km^2 for EP and 104.1×10^3 km^2 for CP; Table 3). A similar analysis to investigate the latitude-altitude relationship was also performed with these data, but no clear changes or improvements were obtained. Based on these results, we deduced that the effect of the choice of lapse rate value is secondary to the quality of overall climate reconstruction within the framework of this study. We acknowledge, however, that the use of a more dynamic determination of lapse rate (and, hence, more adaptive determination of surface air temperature) would lead to a more skilful reconstruction (e.g. Fiddes and Gruber, 2014).

Rock glaciers in the Andes deserve separate attention. In the northern part of the Andes, active rock glaciers are frequently found above 3500 m asl (31°S–35°S) and at 4000-4500 m asl (28°S-30°S) or higher, depending on the region and latitude (Brenning and Trombotto, 2006; Trombotto and Borzotta, 2009; Anetas, 2014; Monnier *et al.*, 2014; Rangecroft *et al.*, 2014). The generation and maintenance of rock glaciers, however, do not necessarily require conditions compatible with purely climate-driven perennial ground freezing (see Trombotto *et al.*, 1999; Trombotto and Ahumada, 2005). Further, the typical spatial scale of rock glaciers (~1.3 km^2, cf. Table 1 of Brenning, 2005) is nearly equivalent to or slightly smaller than that of the ETOPO1 resolution (1 arc-minute), so this downscaling method does not capture the locality of rock glaciers well. The topographic and altitudinal distributions of rock glaciers, however, contain unique climatic information (Kerschner, 1978; Humlum, 1999). Thus, relict rock glaciers could presumably be used as a source of information for regional palaeo-environmental reconstructions. For these reasons, we have carefully examined the inventory of Andean rock glaciers that should serve as indicators for determining or evaluating the occurrence of permafrost in this study. Supplementary Table 1 includes those rock glaciers, the estimated origins of which are either Pleistocene or Holocene (including the Little Ice Age). These sites show results consistent with other previously mentioned evidence (Figures 5 and 6). The rock glaciers as indicators of current permafrost (RG6, RG8, RG10, RG11, RG12, RG15 and

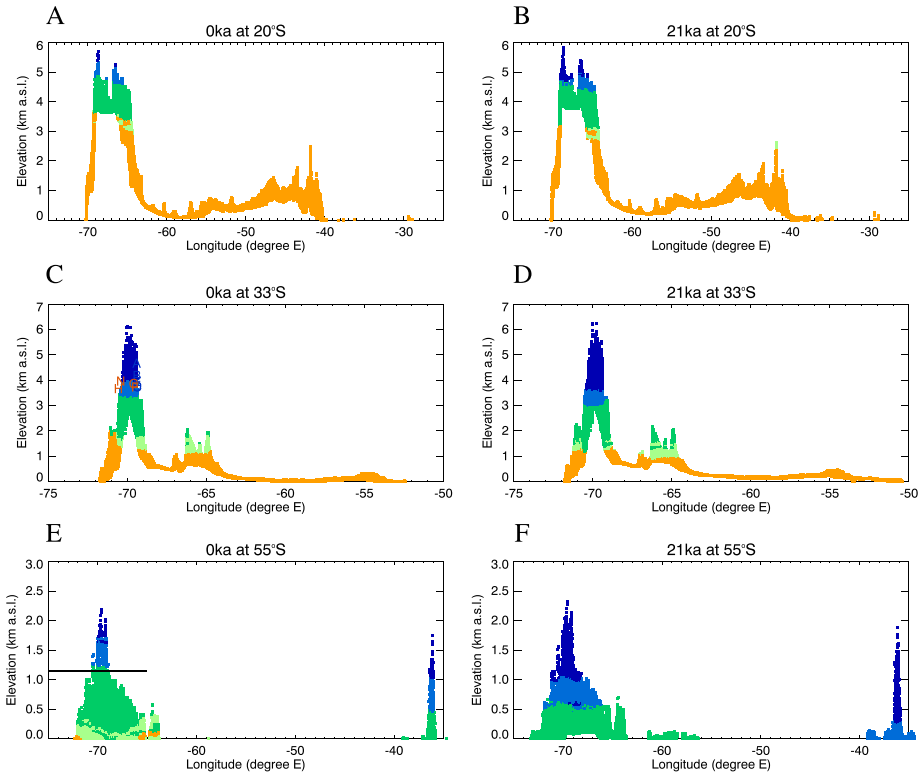

Figure 6 Longitudinal cross-section of frozen ground distribution for (left) 0 ka, and (right) 21 ka periods at 20°S (upper), 33°S (middle) and 55°S (lower) parallels. The colour scheme is the same as given in Figure 3. The horizontal bar in (E) shows the lower limits for mountain permafrost shown in Figure 5. This figure is available in colour online at wileyonlinelibrary.com/journal/ppp

RG16 in Supplementary Table 1) coincide with the lower limit line of intense cryogenic activity, closer to the boundary between the simulated permafrost (blue) and seasonally frozen ground (Sf; green) zones (Figure 5A), while those for the LGM (RG1, RG2, RG3, RG7, RG13 and RG14 in Supplementary Table 1) are found above the lower limit line, only in the midst of the reconstructed Sf zone (Figure 5B).

Longitudinal Cross-Section

Here, we examine cross-sections of frozen ground distribution at different parallels (namely, 1° belts centred at 20°S, 33°S and 55°S) (Figure 6).

Our direct measurements at boreholes on subtropical mountains at 16°S–20°S confirmed the lower limit of present-day permafrost at 5000–5200 m asl, with downscaled boundaries corresponding reasonably well: *c.*5350 m asl between continuous (CP) and discontinuous (EP) permafrost and *c.* 4900 m asl between perennial (CP + EP) and seasonal frost (Sf) on the western cordillera (Figure 6A). These limits descend by about 700 m at 21 ka (Figure 6B). At this latitude, an interesting feature is the occurrence of Sf and If in the Brazilian Highlands above 2500 m asl appearing in the 21 ka downscaled map (around 42°S; Figure 6B), though the occurrence of cryogenic activities in the area is still controversial and under investigation (Clapperton, 1993a).

Altitudinal distribution of moraines observed in the Northern and Central Andes consistently shows that the altitude of the lower limit of cryogenic activities is higher on the western side of the ranges than on the eastern side (Clapperton, 1993a). Present-day reconstruction (Figure 6A) reproduces this longitudinal gradient correctly for all types, though the Late Pleistocene CP (blue) reconstruction at the same latitude (Figure 6B) shows the opposite inclination. In fact, this westerly gradient is not commonly reproduced at other parallels (cf. other plots in Figure 6). That the same atmospheric lapse rate value is used for every grid point and for all periods suggests that the gradient of the lower limit along a parallel line is a reflection of the longitudinal air temperature gradient on an arbitrary horizontal reference level (e.g. mean sea level). Reproducibility of the simulated large-scale atmospheric circulation and resolution of Andean orography in the models may be crucial factors in this regard (cf. the Tibetan Plateau, as noted in Saito *et al.,* 2013a), as large-scale westerlies and moisture differences between the windward and lee sides over the Andes are primarily responsible for the west-east gradient. Examination of overall circulation and moisture flow is beyond the scope of this study, but remains an issue for future research.

For the southern Central Andes (32°S–36°S), the present-day lower limit of Andean permafrost is 3200 m asl around 33°S and 2900 m asl around 36°S according to observations (Trombotto Liaudat *et al.*, 2010, 2014), with some sporadic

occurrences up to about 3700 m asl (representing the boundary between permafrost and non-permafrost sites A to N in Supplementary Table 1). On the other hand, the lower boundary of simulated permafrost is about 3300–3000 m asl (Figure 6C for 33°S). This illustrates the difficulty in determining boundaries, either between active permafrost and relict or past periglacial phenomena, or between perennial and seasonal freezing (cf. Figure 4B). In addition, the subsurface thermal regime at these sites may still be in the process of changing/adapting to the overlying climate (timescale of changes remaining to be investigated, however). For example, site F (Glaciar de Escombros in Supplementary Table 1) showed permafrost at a depth of around 2 m in 2004, though this degraded to no permafrost by the present. For 21 ka (Figure 6D), the lower limit of permafrost in the downscaled map was lowered by 300–400 m, corresponding well to our evidence-based estimate calculated for Laguna del Diamante.

The 55°S cross-section (Figure 6E, F) is presented to illustrate contrasts between Tierra del Fuego (on the continent to the west) and the maritime islands (to the east). The lower limit of the downscaled permafrost zone for the former is about 1200 m asl for the present, whereas the estimation from field observations shows a comparable value, 1000–1300 m asl (Trombotto, 2002; Trombotto Liaudat, 2008). This descends by 650–700 m, to 550 m asl at 21 ka. The Falkland Islands (Islas Malvinas), located north of this latitude line, show only seasonal freezing and no permafrost at 21 ka, as examined above. South Georgia (54°20'S, 36°40'W), in the maritime sub-Antarctic region, is considered to have been widely, if not entirely, covered by ice caps to sea level during the LGM period (Clapperton *et al.*, 1978; Clapperton and Sugden, 1988; Hall K, 2002; Hall B, 2009). Snowfields cover it at present, although the presence of permafrost at higher elevations has been suggested (Thom, 1981). Simulated results show the lower limit of permafrost at around 500 m asl for the present day (Figure 6E), with permafrost reaching almost to sea level for 21 ka (Figure 6F). Since this diagnosis implies only the potential for permafrost, there may still have been no permafrost due to thick ice above ground. As discussed above, the influence of sea ice coverage on the extent of periglacial processes in this island remains for future research.

CONCLUSION

In this study, we attempted to produce the first high-resolution (1 arc-minute) geographical map of frozen ground in South America for the Late Quaternary, especially for the present day and the LGM. A downscaling methodology used for another region (northeastern Asia) proved useful for South America. It enabled a successful reconstruction of present-day Andean permafrost, which the original GCM outputs of coarse resolution could not do. Examinations using fieldwork-based evidence and previous knowledge showed that downscaled maps are largely consistent with existing knowledge of frozen ground. Areas potentially underlain by permafrost at 21 ka (435 000 km^2 in mode) represented about four times those of today's permafrost zone of South America (139 000 km^2), and more than nine times for Patagonia and Tierra del Fuego (12 000 and 110 000 km^2). A potential warm model bias was suspected in the southeastern areas (south of 46°S), including southern Patagonia and the Falkland Islands (Islas Malvinas), where no permafrost was diagnosed in lowland and coastal areas, despite the presence of cryogenic evidence indicating intense freezing (i.e. permafrost or deep seasonal frost) during the Last Glaciation period. Improvement in the overall simulated climate is expected to lead to an improvement in frozen ground classification, especially for coastal lowlands, as well as extra-Andean mountains and highlands on the eastern part of the continent.

ACKNOWLEDGEMENTS

This study was supported by the US National Science Foundation under ARC-1107524. Part of this study was also supported by a grant for collaboration from the Institute of Low Temperature Science at Hokkaido University. We are thankful to Dr Gabriel Goyanes and another reviewer for their constructive criticism for improving the original manuscript. We are also thankful to Dr Nancy Bigelow for discussions and critical reading of the manuscript. The manuscripts have been edited and proofread for language by Nate Bauer, Publications Manager at the International Arctic Research Center, University of Alaska Fairbanks.

REFERENCES

Amante C, Eakins BW. 2009. ETOPO1 1 arc-minute global relief model: procedures, data sources and analysis. NOAA Technical Memorandum NESDIS NGDC-24.

Anetas G. 2014. Contribution à l'étude du permafrost tropical: inventaire des glaciers rocheux de l'Altiplano et de la cordillère occidentale des Andes (Bolivie, Chili). MSc thesis: M2R STADE, Université de Savoie, France.

Benn D, Clapperton C. 2000. Glacial sediment – landform associations and paleoclimate during the last glaciation, Strait of Magellan, Chile. *Quaternary Research* **54**: 13–23.

Bockheim J, Coronato A, Rabassa J, Ercolano B, Ponce J. 2009. Relict sand wedges in southern Patagonia and their stratigraphic and paleo-environmental significance. *Quaternary Science Reviews* **28**: 1188–1199.

Braconnot P, Otto-Bliesner B, Harrison S, Joussaume S, Peterchmitt JY, Abe-Ouchi A, Crucifix M, Driesschaert E, Fichefet T, Hewitt CD, Kageyama M, Kitoh A, Laîné A, Loutre MF, Marti O, Merkel U, Ramstein G, Valdes P, Weber SL, Yu Y, Zhao Y. 2007. Results of PMIP2 coupled simulations of the Mid-Holocene and Last Glacial Maximum – part 1: experiments and large-scale features. *Climate of the Past* **3**: 261–277.

Braconnot P, Harrison SP, Kageyama M, Bartlein PJ, Masson-Delmotte V, Abe-Ouchi A, Otto-Bliesner B, Zhao Y. 2012. Evaluation

of climate models using palaeoclimatic data. *Nature Climate Change* **2**: 417–424. DOI: 10.1038/NCLIMATE1456.

Brenning A. 2005. Geomorphological, Hydrological and Climatic Significance of Rock Glaciers in the Andes of Central Chile (33–35°S). *Permafrost and Periglacial Processes.* **16**: 231–240. DOI:10.1002/ppp.528.

Brenning A, Trombotto D. 2006. Logistic regression modeling of rock glacier and glacier distribution: topographic and climatic controls in the semi-arid Andes. *Geomorphology* **81**: 141–154. DOI:10.1016/j.geomorph.2006.04.003.

Brown J, Ferrians OJ, Jr, Heginbottom JA, Melinikov ES. 1997. Circum-Arctic Map of Permafrost and Ground-Ice Conditions, USGS Circum-Pacific Map Series, Map CP-45, US Department of the Interior.

Clapperton C. 1993a. *Quaternary Geology and Geomorphology of South America*. Elsevier: London.

Clapperton C, Sugden D. 1988. Holocene glacier fluctuations in South America and Antarctica. *Quaternary Science Reviews* **7**: 185–198.

Clapperton C, Sugden D, Birnie RV, Hansom J, Thom G. 1978. Glacier fluctuations in South Georgia and comparison with other island groups in the Scotia Sea. In *X INQUA Congress Antarctic Glacial History and World Paleoenvironments*, Van Zinderen Bakker EM (ed). Balkema: Rotterdam; 98–104.

Clapperton CM. 1993b. Nature of environmental changes in South America at the Last Glacial Maximum. *Palaeogeography, Palaeoclimatology, Palaeoecology* **101**: 189–208.

Clark PU, Mix AC. 2002. Ice sheets and sea level of the Last Glacial Maximum. *Quaternary Science Reviews* **21**: 1–7.

Coronato C, Rabassa J. 2007. Late Quaternary in South America. In *Encyclopedia of Quaternary Science*, Elias S (ed). Elsevier: Amsterdam; vol. **2**: 1101–1109.

Corte A. 1997. *Geocriología. El Frío en la Tierra*. Ediciones Culturales de Mendoza, Fundar Editorial Gráfica: Mendoza.

Corte AE. 1953. Contribución a la Morfología Periglacial de la Alta Cordillera con Especial Mención del Aspecto Criopedológico. *Anales del Departamento de Investigaciones Científicas* 1.

Corte AE. 1986. Delimitation of geocryogenic (periglacial) regions and associated geomorphic belts at 33°S, Andes of Mendoza, Argentina. *Biuletyn Periglacjlny* **31**: 32–34.

Corte AE. 1991. Chronostratigraphic correlations of cryogenic episodes in Central Andes and Patagonia. *Permafrost and Periglacial Processes* **2**: 67–70. DOI:10.1002/ppp.3430020111.

Fiddes J, Gruber S. 2014. TopoSCALE v.1.0: downscaling gridded climate data in complex terrain. *Geoscientific Model Development* **7**: 387–405. DOI:10.5194/gmd-7-387-2014.

French HM. 2007. *The periglacial environment*, Third edition. John Wiley and Sons: Chichester.

Garleff K, Stingl H. 1986. Geomorphologische Aspekte aktuellen und vorzeitlichen Permafrostes in Argentinien. Zentralblatt für Geologie und Palaeontologie, Teil I. *Allgemeine, Angewandte, Regionale und Historische Geologie* **9–10**: 1367–1374.

Gersonde R, Crostab X, Abelmanna A, Armand L. 2005. Sea-surface temperature and sea ice distribution of the Southern Ocean at the EPILOG Last Glacial Maximum—a circum-Antarctic view based on siliceous microfossil records. *Quaternary Science Reviews* **24**: 869–896.

Goyanes G, Massabie A. 2015. Push moraines in the upper valley of Santa Cruz river, southwest Argentina. Structural analysis and relationship with Late Pleistocene paleoclimate. *Journal of South American Earth Sciences* **57**: 1–11.

Hall K. 2002. Review of present and Quaternary periglacial processes and landforms of the maritime and sub-Antarctic region. *South African Journal of Science* **98**: 71–81.

Hall B. 2009. Holocene glacial history of Antarctica and the sub-Antarctic islands. *Quaternary Science Reviews* **28**: 2213–2230. DOI:10.1016/j.quascirev.2009.06.011.

Heusser C. 1991. Biogeographic evidence for Late Pleistocene paleoclimate of Chile. *Bamberger Geographische Schriften* **11**: 257–270.

Heusser CJ. 2003. *Ice Age Southern Andes – A chronicle of paleoecological events*. Elsevier: Amsterdam.

Hubbard A, Hein AS, Kaplan MR, Hulton NRJ, Glasser N. 2005. A Modelling reconstruction of the Last Glacial Maximum ice sheet and its deglaciation in the vicinity of the northern Patagonian icefield, South America. *Geografiska Annaler: Series A, Physical Geography* **87**: 375–391. DOI: 10.1111/j.0435-3676.2005.00264.x.

Hulton NRJ, Purves RS, McCulloch RD, Sugden DE, Bentley MJ. 2002. The Last Glacial Maximum and deglaciation in southern South America. *Quaternary Science Reviews* **21**: 233–241.

Humlum O. 1999. The Climatic Significance of Rock Glaciers. *Permafrost and Periglacial Processes* **9**(4): 375–395.

Intergovernmental Panel on Climate Change. 2013. Climate Change 2013: The Physical Science Basis. *Contribution of Working Group I to the Fifth Assessment Report of the Intergovernmental Panel on Climate Change*, Stocker TF, Qin D, Plattner G-K, Tignor M, Allen SK, Boschung J, Nauels A, Xia Y, Bex V, Midgley PM (eds). Cambridge University Press: Cambridge; 383–464.

Kerschner H. 1978. Palaeoclimatic inferences from late Würm rock glaciers, Eastern Central Alps, Western Tyrol, Austria. *Arctic and Alpine Research* **10**: 635–644.

Levavasseur G, Vrac M, Roche DM, Paillard D, Martin A, Vandenberghe J. 2011. Present and LGM permafrost from climate simulations: contribution of statistical downscaling. *Climate of the Past* **7**: 1225–1246.

Lliboutry L. 1998. Glaciers of South America – Glaciers of Chile and Argentina. In *Satellite Image Atlas of Glaciers of the World: South America, United States Geological Survey*, Williams R, Ferrigno J (eds). Professional Paper, 1386-I: Washington; 109–206.

Markgraf V. 1989. Palaeoclimates in the Central and South America since 18,000 BP based on pollen and lake-level records. *Quaternary Science Reviews* **8**: 1–24.

Markgraf V. 1991. Late Pleistocene environmental and climatic evolution in southern South America. *Bamberger Geographische Schriften* **11**: 271–281.

Milne GA, Mitrovica JX. 2008. Searching for eustasy in deglacial sea-level histories. *Quaternary Science Reviews* **27**: 2292–2302.

Modenesi M. 1992. Depósitos de Vertente e Evolução Quaternária do Planalto do Itatiaia. *Revista do Instituto Geológico* **13**: 31–46.

Monnier S, Kinnard C, Surazakov A, Bossy W. 2014. Geomorphology, internal structure, and successive development of a glacier foreland in the semiarid Chilean Andes (Cerro Tapado, upper Elqui Valley, 30°08'S., 69°55'W.). *Geomorphology* **207**: 126–140.

Péwé T. 1969. The periglacial environment. In *The Periglacial Environment*, Péwé T (ed). Mc Gill-Queen's University Press: Montreal; 1–10.

Rangecroft S, Harrison S, Anderson K, Magrath J, Castel AP, Pacheco P. 2014. A First Rock Glacier Inventory for the Bolivian Andes. *Permafrost and Periglac. Process*. DOI:10.1002/ppp.1816.

Romanovskij N. 1973. Regularities in Formation of Frost-Fissures and Development of Frost-Fissure Polygons. *Biul. Peryglacjalny* **23**: 237–277.

Saito K, Sueyoshi T, Marchenko S, Romanovsky V, Otto-Bliesner B, Walsh J, Bigelow N, Hendricks A, Yoshikawa K.

2013a. LGM permafrost distribution: How well can the latest PMIP multi-model ensembles perform reconstruction? *Climate of the Past* **9**: 1697–1714. DOI:10.5194/cp-9-1697-2013.

Saito K, Zhang T, Yang D, Marchenko S, Barry RG, Romanovsky V, Hinzman L. 2013b. Influence of the Physical Terrestrial Arctic in the Eco-climate System. *Ecological Applications* **23**: 1778–1797. DOI:10.1890/11-1062.1.

Saito K, Marchenko S, Romanovsky V, Hendricks A, Bigelow N, Yoshikawa K, Walsh J. 2014. Evaluation of LPM permafrost distribution in northeast Asia reconstructed and downscaled from GCM simulations. *Boreas* **43**: 733–749. DOI:10.1111/bor.12038.

Schellmann G, Wenzens G, Radtke U, Trombotto D, Zárate M, Schnack E. 2000. Landscape Evolution of Southern Patagonia. In *Zeitschrift für Angewandte Geologie*, Sonderheft, SH 1, Miller H, Herbé F (coords). Schweizerbart'sche Verlagsbuchhandlung: Stuttgart; 63–68.

Schubert C, Clapperton CM. 1990. Quaternary glaciations in the northern Andes (Venezuela, Colombia and Ecuador). *Quaternary Science Reviews* **9**: 123–135.

Skvarca P. 2002. Importancia de los glaciares del Hielo patagónico Sur para el desarrollo regional. In *Relatorio del XV Congreso Geológico Argentino 5, Geología y Recursos Naturales de Santa Cruz,* Haller MJ (ed). El Calafate: Buenos Aires; vol. **1**; 785–798.

Thom G. 1981. Patterned ground in South Georgia. PhD thesis, University of Aberdeen, Scotland.

Trombotto D. 1991. Untersuchungen zum periglazialen Formenschatz und zu periglazialen Sedimenten in der Lagunita del Plata, Mendoza, Argentinien. *Heidelberger Geographische Arbeiten* **90**: 1–171.

Trombotto D. 1994. El Permafrost Patagónico Pasado. *Revista del Museo de Historia Natural de San Rafael* **12**: 229–249.

Trombotto D. 1996. Fossiler kryogener Formenschatz des südlichen Südamerika. ("Fossil cryogenic forms of Southern South America"). *Zeitschrift für Geomorphologie* N.F., Suppl.-Bd. **104**: 175–186.

Trombotto D. 2000. Survey of Cryogenic Processes, Periglacial Forms and Permafrost Conditions in South America. *Revista do Instituto Geológico* **21**: 33–55.

Trombotto D. 2002. Inventory of fossil cryogenic forms and structures in Patagonia and the mountains of Argentina beyond the Andes. *South African Journal of Science* **98**: 171–180.

Trombotto D. 2003. Mapping of permafrost and the periglacial environment, Cordón del Plata, Argentina. In *8th International Conference on Permafrost. Permafrost, Extended Abstracts*, Haeberli W, Brandová D (eds). Zurich, Switzerland; 161–162.

Trombotto D, Ahumada AL. 2005. Los Fenómenos Periglaciales. Identificación, Determinación y Aplicación. *Opera Lilloana* 45. Fundación "Miguel Lillo": San Miguel de Tucumán, Argentina.

Trombotto D, Borzotta E. 2009. Indicators of present global warming through changes in active layer-thickness, estimation of thermal diffusivity and geomorphological observations in the Morenas Coloradas rock glacier, Central Andes of Mendoza, Dry Andes, Argentina. *Cold Regions Science and Technology* **55**: 321–330.

Trombotto D, Stein B. 1993. El último criómero pleistocénico en la región de los "kopjes" y de las grandes mesetas, Patagonia, Argentina. In *XII Congreso Geológico Argentino, Actas*, Mendoza; Akian Gráfica Editora: Buenos Aires, Argentina; Vol. **VI**; 92–96.

Trombotto D, Buk E, Hernández J. 1999. Rock glaciers in the Southern Central Andes (approx. 33°S–34°S). Mendoza, Argentina: a review. *Bamberger Geographische Schriften* **19**: 145–173.

Trombotto Liaudat D. 2008. Geocryology of Southern South America. In *The Late Cenozoic of Patagonia and Tierra del Fuego*, Rabassa J (ed). Elsevier: Amsterdam; vol. **11**; 255–268.

Trombotto Liaudat D, Travassos J, Ahumada AL, Bodin X, Brenning A, Gomez PC, Francou B, Götz J, Palacios D. 2010. Monitoring sites and recent studies of periglacial processes and landforms in South America. In *IPY Oslo Science Conference*, Jun 2010, Oslo, Norway.

Trombotto Liaudat D, Penas P, Aloy G. 2014. Impact of volcanic processes on the cryospheric system of the Peteroa Volcano, Andes of southern Mendoza, Argentina. *Geomorphology* **208**: 74–87.

University of East Anglia Climatic Research Unit, Jones PD, Harris I. 2013. CRU TS3.20: Climatic Research Unit (CRU) Time-Series (TS) Version 3.20 of High Resolution Gridded Data of Month-by-month Variation in Climate (Jan. 1901 - Dec. 2011). NCAS British Atmospheric Data Centre. http://catalogue.ceda.ac.uk/uuid/2949a8a25b375c9e323c53f6b6cb2a3a [27 November 2014]

Vandenberghe J, Renssen H, Roche DM, Goosse H, Velichko AA, Gorbunov A, Levavasseur G. 2012. Eurasian permafrost instability constrained by reduced sea-ice cover. *Quaternary Science Reviews* **34**: 16–23.

Vandenberghe J, French HM, Gorbunov A, Marchenko S, Velichko AA, Jin H, Cui Z, Zhang T, Wan X. 2014. The Last Permafrost Maximum (LPM) map of the Northern Hemisphere: permafrost extent and mean annual air temperatures, 25–17 ka BP. *Boreas* **43**: 652–666. DOI: 10.1111/bor.12070.

World Glacier Monitoring Service and the National Snow and Ice Data Center. 1999, updated 2012. *World Glacier Inventory*. National Snow and Ice Data Center: Zurich, Switzerland and Boulder, Colorado. DOI: 10.7265/N5/NSIDC-WGI-2012-02

SUPPORTING INFORMATION

Additional supporting information may be found in the online version of this article at the publisher's web site.